Scientia Iranica B (2021) 28(4), 2176–2186

Sharif University of Technology
Scientia Iranica
Transactions B: Mechanical Engineering
http://scientiairanica.sharif.edu

A particle method development for analyzing the post-buckling behavior of composite plates with a cut-out

M. Dehghani*

Department of Mechanical Engineering, Yazd University, Yazd, Postal code 89195-741 Iran.

Received 28 May 2020; received in revised form 3 October 2020; accepted 3 May 2021

KEYWORDS
Perforated composite plates;
Buckling;
Post-buckling;
Particle Semi-Energy (PSE);
Elliptical and circular cut-outs.

Abstract. The present study investigates nonlinear buckling and post-buckling behaviors of composite plates with the circular/elliptical cut-out using Particle Semi-Energy (PSE) method. The semi-energy is based on the solution of the compatibility equation obtained from an Airy force and out-of-plane displacement functions. The unknown parameters of these functions were determined by minimizing the potential energy. The integrals of the potential energy were then replaced by the summations at the perforated plate particle (node). The cut-out was easily modeled using these nodes. This method enjoys some advantages, namely easy cut-out modeling by nodes and proposing just one of the displacement fields (i.e., out-of-plane). According to the results, there was good agreement (1.25%) between the post-buckling loads derived from PSE in this paper and the experimental test of the literature. According to the experimental test results, the accuracy of Finite Element Method (FEM) was 7.5%. This study also evaluated the effects of rotating the elliptical cut-out and replacing it with two other circular cut-outs in the same areas on the post-buckling load.

1. Introduction

Composite materials are among the most useful engineering structures that are preferred over other common materials owing to their desirable structural properties such as higher specific strength and lightness. This study suggests a new technique in the semi-energy method for nonlinear post-buckling analysis of composite plates with cut-outs.

The buckling and post-buckling behaviors of the composite laminates containing a cut-out were developed using Semi-Energy Finite Strip Method (SE-FSM) [1]. Based on Lagrangian strain, the strains of the composite plate were defined that comprised both linear and nonlinear displacement fields. According to the semi-energy method [2], the shape function for the out-of-plane displacement was set as the trigonometric functions based on the boundary conditions of plate edges in the longitudinal direction and Hermitian polynomial was used in transverse direction of the plate. The in-plane forces were defined as the differential of Airy force functions. Having been substituted into von Kármán's compatibility equation, these Airy functions became related to out-of-plane displacement. Then, the in-plane displacement fields were achieved based on the strain definition using out-of-plane displacement and Airy functions. The non-linear equilibrium equations were derived through minimizing the potential energy. The governing equations of the equilibrium were solved using the Newton-Raphson technique. To

*. *Tel.: +98 35 31232222*
E-mail addresses: mo.dehghani@stu.yazd.ac.ir and muh.dehghani@gmail.com

doi: 10.24200/sci.2021.55993.4506

model the cut-out, the plate was divided by strips and semi-energy method was applied to the strips. The potential energy of the cut-out was not added to the whole potential energy of the incomplete strips placed in the cut-out region. Moreover, SE-FSM was employed to evaluate the effects of the stiffener on the post-buckling behavior of composite laminates with circular cut-out [3]. The potential energy of the planer and ring types of stiffener was added to the whole potential energy of the strips placed in the stiffener region. The numerical results were validated by the experimental tests. Although the end-shortening capacity of plates with a planer stiffener is the highest, this plate has the lowest buckling load compared to the plate with ring and longitudinal types of stiffener. The buckling load of the plate with a longitudinal type of stiffener is the highest.

Numerical buckling analysis of carbon fibre-epoxy composite plates with one, two, and three central rectangular cut-outs was carried out [4]. The areas allocated to all types of cut-outs were equal. Linear and nonlinear Finite Element Methods (FEMs) were employed to model the buckling state using the elastic composite plate elements. The results were validated by the experimental test [5]. Increasing the number of rectangular cut-outs with constant area summation would increase maximum buckling load and decrease maximum deflection.

The post-buckling behavior of relatively thick composite plates with circular/elliptical holes was investigated using full energy method as well as the first-order shear deformation plate theory [6]. Defined based on Green strain [7], the strains of the composite plate are characterized by both linear and nonlinear displacement fields and size-dependent effect of the plate thickness. The out-of-plane shear strain added to the strain field corresponds to the first-order shear deformation plate theory. According to full energy method [8], the shape functions for the in- and out-of-plane displacements fields as well as the rotations of a strip edges were set as trigonometric functions based on boundary conditions of plate edges. The non-linear equilibrium equations were derived from minimizing the potential energy. The governing equations of the equilibrium were solved by the Newton-Raphson technique. In this study, the continuous integrals of the potential energy were replaced by summations calculated over all nodes on the perforated plate. Nodes were selected based on Gauss-Chebyshev quadrature. To this end, three different types of boundary conditions were employed. All types were featured based on a simple support boundary condition along the axial loading. One of the longitude edges was simple/clamp and the other was simple/free. The post-buckling results and buckling loads were validated using FEM and experimental results, respectively [9]. In case the four boundaries are simple, the buckling load of the plate with the elliptical cut-out aligned in the loading direction is lower than that of the plate with a vertical elliptical cut-out. This result varies in other boundary conditions [10].

The post-buckling of the relatively thick functionally-graded plates with square and rectangular cut-outs was investigated using full energy method and first-order shear deformation plate theory [11]. The plate was modeled by assembling eight plate elements placed around the cut-out. This modeling was called Penalty method. The strains and shape functions of the displacement and rotations of eight plate elements were similar to those reported in the research [6]. The free boundary conditions were first considered in the Ritz approximation for the sharing edges between the adjoining elements. The non-linear equilibrium equations were derived in [6] and the continuous integrals of the potential energy were replaced by summations calculated over all nodes in the eight plate elements. The governing equations of equilibrium were solved using the quadratic extrapolation technique. Moreover, FEM was employed to validate the results of this study.

The buckling load parameters for the functionally graded carbon nanotube sandwich structure were investigated using numerical method. The plate was under the compression loading [12] as well as the uniform [13–15] and non-uniform [14,16–18] thermal loading. The temperature profile was assumed to linearly [16] and nonlinearly [17] increase from the bottom surface at room temperature to the top surface of the composite plate. Further, the free vibration fundamental frequency of this structure under uniform thermal loading was obtained [19,20]. A higher-order polynomial displacement with nine unknown parameters [12–19,21] and low-order polynomial displacement [20] was used to calculate the global mid-plane displacement. The mechanical and thermal strain vectors were defined in the form of nodal displacement vector via Green-Lagrange assumption. The governing equilibrium equation was derived by the variational principle. The total strain energy and the work done due to temperature rise were also calculated. This equilibrium equation was rearranged in the form of eigenvalue and eigenvectors, and the subsequent algebraic form was achieved through the iso-parametric displacement finite element steps. The spherical geometry represented the highest critical buckling temperature. The uniform critical buckling temperature decreased following an increase in the length-to-thickness and curvature ratios of the plate.

In the literature, the post-buckling of composite plates was analyzed using full-energy and semi-energy method. These methods were then applied to the whole plate analytically or to the strips and elements

numerically. The accuracy of the full-energy method was lower than that of the semi-energy method, mainly because the former set the shape functions to all displacement and the latter just set the shape function for out-of-plane displacement, and other ones were derived using strain definition and Airy function. The Airy functions satisfied the compatibility equations. In the strip modeling [1], the circular cut-out was modeled as the summation of some small rectangles. Calculating the potential energy integration of each strip requires a considerable amount of time. Increasing the number of strips approximately would change the rectangular cut-out shape to the ideal circle, as shown in [22]; however, solving the integration still requires much time. The error of FEM was higher than that of the semi-energy method [1].

The present study aimed to investigate the post-buckling behavior of composite laminates containing a circular/elliptical cut-out using Particle Semi-Energy (PSE) method and classical plate theory. To this end, a shape function was set to out-of-plane displacement based on the boundary condition. In-plane displacements were then derived using strain definition and Airy function. The non-linear equilibrium equations were also obtained through minimizing the potential energy. The continuous integrals of the potential energy were replaced by summations calculated over all nodes in the perforated plate. The governing equilibrium equations were finally solved through the Newton-Raphson technique. Further, the buckling loads were calculated by increasing the end-shortening capacity. The results were validated using the experimental tests [1] and FEM.

2. Basic formulation of composite laminate

The strains of the composite plate are defined based on Lagrangian strain containing the linear and nonlinear displacement fields:

$$\varepsilon = \left\{ \begin{array}{c} \varepsilon_x \\ \varepsilon_y \\ \varepsilon_{xy} \end{array} \right\} = \varepsilon^L + \varepsilon^{NL}, \tag{1}$$

where:

$$\varepsilon^L = \left\{ \begin{array}{c} \frac{\partial u}{\partial x} \\ \frac{\partial v}{\partial y} \\ \frac{1}{2}\left(\frac{\partial u}{\partial y} + \frac{\partial v}{\partial x}\right) \end{array} \right\},$$

$$\varepsilon^{NL} = \left\{ \begin{array}{c} \frac{1}{2}\left(\frac{\partial w}{\partial x}\right)^2 \\ \frac{1}{2}\left(\frac{\partial w}{\partial y}\right)^2 \\ \frac{1}{2}\left(\frac{\partial w}{\partial x}\frac{\partial w}{\partial y}\right) \end{array} \right\}, \tag{2}$$

and u, v are in-plane and w the out-of-plane displacements. The strain-displacement relations (1) satisfy the compatibility equation as follows:

$$\frac{\partial^2 \varepsilon_x}{\partial y^2} + \frac{\partial^2 \varepsilon_y}{\partial x^2} - \frac{\partial^2 \gamma_{xy}}{\partial x \partial y} = \left(\frac{\partial^2 w}{\partial x \partial y}\right)^2 - \left(\frac{\partial^2 w}{\partial y^2}\right)\left(\frac{\partial^2 w}{\partial x^2}\right). \tag{3}$$

Generalized Hook's equation for a composite laminate is formulated as Eq. (4).

$$\begin{bmatrix} \varepsilon \\ M \end{bmatrix} = \begin{bmatrix} A^* & B^* \\ B^* & D^* \end{bmatrix} \begin{bmatrix} N \\ \kappa \end{bmatrix}, \tag{4}$$

$$N = \left\{ \begin{array}{c} N_x \\ N_y \\ N_{xy} \end{array} \right\}, \quad M = \left\{ \begin{array}{c} M_x \\ M_y \\ M_{xy} \end{array} \right\}, \quad \kappa = \left\{ \begin{array}{c} \kappa_x \\ \kappa_y \\ \kappa_{xy} \end{array} \right\}, \tag{5}$$

where κ, N, and M are the curvature of the neutral plane of composite element, forces, and moments per unit length acting on the component of the element, respectively. The curvatures are defined based on out-of-plane displacement derivations $\kappa_x = \left(\partial^2 w/\partial x^2\right), \kappa_y = \left(\partial^2 w/\partial y^2\right), \kappa_{xy} = 2\left(\partial^2 w/\partial x \partial y\right)$. The coefficient matrices are derived as $A^* = A^{-1}, B^* = -A^{-1}.B, H^* = B.A^{-1}, D^* = D - B.A^{-1}.B$. The matrix A is the in-plane stiffness matrix of the composite material, B the coupling matrix of the forces imposed on the in- and out-of-plane moments, and D the stiffness of moments as well as the curvatures of the element. The matrices A, B, and D were determined in Ref. [1].

The forces per unit length acting on the component of the element are expressed in Eq. (6) based on the Airy force function (F) derivations:

$$N_x = \frac{\partial^2 F}{\partial y^2}, \quad N_y = \frac{\partial^2 F}{\partial x^2}, \quad N_{xy} = -\frac{\partial^2 F}{\partial x \partial y}. \tag{6}$$

Given that the matrix $B^* = 0$ and $A^*_{13} = A^*_{23} = 0$ for the symmetrical laminate, by substituting Eq. (4) and definitions of Eq. (6) into Eq. (3), the compatibility equation deforms as obtained by Eq. (7):

$$A^*_{22}\frac{\partial^4 F}{\partial x^4} + \left(2A^*_{12} + A^*_{33}\right)\frac{\partial^4 F}{\partial x^2 \partial y^2} + A^*_{11}\frac{\partial^4 F}{\partial y^4} = \left(\frac{\partial^2 w}{\partial x \partial y}\right)^2 - \left(\frac{\partial^2 w}{\partial x^2}\right)\left(\frac{\partial^2 w}{\partial y^2}\right). \tag{7}$$

In the case of the out-of-plane displacement (w), the Airy function is derived by solving the partial Eq. (7), and the buckling load (N_x) is calculated through the derivation of function F using Eq. (6).

3. Semi-energy formulation

A shape function for out-of-plane displacement is set based on the boundary conditions, and in-plane displacements are derived from the means of Airy functions. These functions satisfy the in-plane boundary condition and compatibility equation.

The plate is clamped at both ends (i.e., at ends $x = 0$ and L in Figure 1) and loaded to a uniform

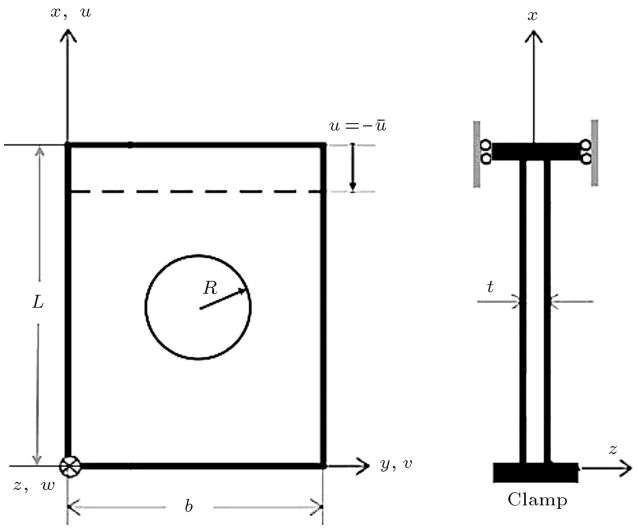

Figure 1. Description of the boundary conditions of a perforated plate subjected to a prescribed uniform end-shortening.

end shortening $\bar{u}$ at end $x = L$ only. The boundary conditions for the plate including a circular cut-out are summarized as follows:

$$\begin{cases} w = \frac{\partial w}{\partial x} = 0 \quad \text{at} \quad x = 0, L \\ u = \begin{cases} 0 & \text{at} \quad x = 0 \\ -\bar{u} & \text{at} \quad x = L \end{cases} \end{cases} \tag{8}$$

According to the boundary conditions of Eq. (8), the out-of-plane displacement field is proposed in Eq. (9), where w_1 is the maximum deflection of plate which will be determined later.

$$w = w_1 \cos(nx), \qquad n = \frac{2m\pi}{L}. \tag{9}$$

The compatibility equation is satisfied by substituting the out-of-plane displacement of Eq. (9) into Eq. (7), as shown in the following:

$$A^*_{22}\frac{\partial^4 F}{\partial x^4} + (2A^*_{12} + A^*_{33})\frac{\partial^4 F}{\partial x^2 \partial y^2} + A^*_{11}\frac{\partial^4 F}{\partial y^4} = 0. \tag{10}$$

The suitable Airy function F can be assumed as follows:

$$F(x, y) = F_0(y) + F_n(y)\cos(nx). \tag{11}$$

By substituting Eq. (11) into Eq. (10), two fourth-order ordinary differential equations are derived as follows:

$$\mathrm{A}^*_{11}\frac{d^4 F_0}{dy^4} = 0,$$

$$\mathrm{A}^*_{11}\frac{d^4 F_n}{dy^4} - n^2(2\mathrm{A}^*_{12} + \mathrm{A}^*_{33})\frac{d^2 F_n}{dy^2} + n^4 \mathrm{A}^*_{22} F_n = 0. \tag{12}$$

The solution of the first equation is a third-order polynomial equation. The solution of the second equation depends on the sign of *Delta* ($\Delta = (2A^*_{12} + A^*_{33})^2 - 4A^*_{11}A^*_{22}$) [8]. If the sign of *Delta* is positive, the solution form will be:

$$\begin{aligned} F_n =& C_1 \cosh(M) + C_2 \sinh(M) \\ &+ C_3 \cosh(N) + C_4 \sinh(N), \\ M =& n\frac{\sqrt{2A^*_{12} + A^*_{33} + \sqrt{\Delta}}}{2A^*_{11}}, \\ N =& n\frac{\sqrt{2A^*_{12} + A^*_{33} - \sqrt{\Delta}}}{2A^*_{11}}. \end{aligned} \tag{13}$$

The unknown coefficients C_1 to C_4 will be later expressed based on the in-plane displacements. To find the axial displacement, the first row of Eq. (1) is written again in Eq. (14). The Eqs. (4), (9), and (11) are then substituted into the new form of Eq. (1) as shown in the following:

$$\begin{aligned} \frac{\partial u}{\partial x} &= \varepsilon_x - \frac{1}{2}\left(\frac{\partial w}{\partial x}\right)^2 \\ &= A^*_{11}N_x + A^*_{12}Ny - \frac{1}{2}\left(\frac{\partial w}{\partial x}\right)^2 \\ &= A^*_{11}\frac{\partial^2 F}{\partial y^2} + A^*_{12}\frac{\partial^2 F}{\partial x^2} - \frac{1}{2}\left(\frac{\partial w}{\partial x}\right)^2 \\ &= \left(A^*_{11}\frac{\partial^2 F_n}{\partial y^2} - n^2 A^*_{12}F_n\right)\cos(nx) \\ &\quad + A^*_{11}\frac{\partial^2 F_0}{\partial y^2} - \frac{w_1^2 n^2}{8}(1 - \cos(2nx)). \end{aligned} \tag{14}$$

The axial displacement Eq. (15) is obtained by integrating Eq. (14) with the boundary conditions of Figure 1:

$$\begin{aligned} u &= f_u \sin(nx) + \frac{w_1^2 n}{16}\sin(2nx) - \frac{\bar{u}}{L}x, \\ f_u &= \frac{1}{n}\left(A^*_{11}\frac{\partial^2 F_n}{\partial y^2} - n^2 A^*_{12}F_n\right), \end{aligned} \tag{15}$$

while $\partial^2 F_0/\partial y^2 = -\left(\bar{u}/L - w_1^2 n^2/8\right)/A^*_{11}$. Moreover, Eqs. (4), (9), and (11) should be substituted into the new form of the second row of Eq. (1) to find the transverse displacement.

$$\begin{aligned} \frac{\partial v}{\partial y} &= \varepsilon_y - \frac{1}{2}\left(\frac{\partial w}{\partial y}\right)^2 \\ &= A^*_{21}\frac{\partial^2 F}{\partial y^2} + A^*_{22}\frac{\partial^2 F}{\partial x^2} - \frac{1}{2}\left(\frac{\partial w}{\partial y}\right)^2 \\ &= \left(A^*_{21}\frac{\partial^2 F_n}{\partial y^2} - n^2 A^*_{22}F_n\right)\cos(nx) + A^*_{21}\frac{\partial^2 F_0}{\partial y^2}. \end{aligned} \tag{16}$$

Eq. (17) for the transverse displacement is derived from integrating Eq. (16) by means of the value of sentence $\left(n^2 A^*_{22} F_n\right)$ with the compatibility Eq. (12).

$$v = -\frac{A^*_{12}}{A^*_{11}}\left(\bar{u} - \frac{w_1^2 n^2}{8}\right) + f_v \cos(nx) - f_v|_{y=0},$$

$$f_v = \left(\frac{A^*_{11}}{n^2}\frac{\partial^3 F_n}{\partial y^3} - (A^*_{12} + A^*_{33})\frac{\partial F_n}{\partial y}\right). \quad (17)$$

The unknown coefficients C_1 to C_4 are determined by Eq. (18):

$$f_u|_{y=0} = u_1, \qquad f_u|_{y=b} = u_2,$$

$$f_v|_{y=0} = v_1, \qquad f_v|_{y=b} = v_2, \quad (18)$$

where (u_1, v_1) and (u_2, v_2) are the displacement vectors of the plate edges at $y = 0$ and $y = b$, respectively, which will be determined later by solving the non-linear equilibrium equations derived from minimizing the potential energy. The potential energy of the symmetric composite plate is given in Eq. (19):

$$U = \frac{1}{2}\iint_{\Omega}\left(\left\{\varepsilon^L + \varepsilon^{NL}\right\}^T A\left\{\varepsilon^L + \varepsilon^{NL}\right\} + \kappa^T D\kappa\right), \quad (19)$$

where Ω is the area with a cut-out in the plate. In case the perforated plate is divided by nodes, as shown in Figure 2, the integral in Eq. (19) should be replaced by summation in Eq. (20).

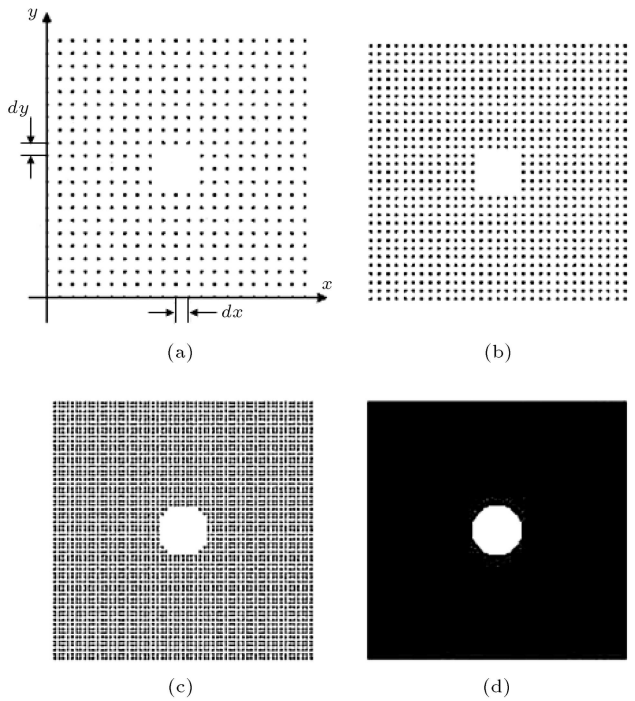

Figure 2. The node configurations of summation potential energy shown on the plate including a circular cut-out with the radius R, while the distances between the nodes are (a) $R/2$, (b) $R/3$, (c) $R/6$, and (d) $R/12$.

$$U = \frac{1}{2}\sum_i\sum_j\left(\left\{\varepsilon^L + \varepsilon^{NL}\right\}^T A\left\{\varepsilon^L + \varepsilon^{NL}\right\} + \kappa^T D\kappa\right)\Omega_{ij}, \quad (20)$$

where $\Omega_{ij} = dx \times dy$ is the area around the node at the position (i, j).

The non-linear equilibrium equations are obtained from minimizing the potential energy. The governing equilibrium equations are solved using the Newton-Raphson technique:

$$K(d_k)\,\Delta d_k = -R(d_k),$$

$$d_{k+1} = \Delta d_k + d_k, \quad (21)$$

where:

$$d^T = [d_1, d_2, d_3, d_4, d_5] = [w_1,\ u_1,\ u_2,\ v_1,\ v_2],$$

$$R(d_{kk}) = \frac{\partial U}{\partial d_k}, \quad K(d_{kl}) = \frac{\partial U}{\partial d_k \partial d_l},$$

$$k, l = 1, 2, 3, 4, 5. \quad (22)$$

By integrating the axial force upon the perforated plate surface, the total mean force imposed on the composite plate with a cut-out can be obtained as follows:

$$N = \frac{\left(\iint_{\Omega}\left(A\left\{\varepsilon^L + \varepsilon^{NL}\right\}\right)dxdy\right)}{L} = \frac{\sum_i\sum_j A\left\{\varepsilon^L + \varepsilon^{NL}\right\}\Omega_{ij}}{L}. \quad (23)$$

The flowchart of PSE method for the buckling and post-buckling analyses of the composite plate with a cutout is presented in Figure 3.

4. Finite Element Method (FEM)

Based on the plate configuration in Figure 1, FEM is proposed in Figure 4(a). In addition, linear and nonlinear analyses were employed to determine the buckling and post-buckling behaviors of the plate, respectively. In this modeling, the plate element shown in Figure 4(b) was used which itself was taken from the ANSYS software instructions. The element has eight nodes (I, J, K, L, M, N, O, and P), each with six degrees of freedom (three degrees of displacement and three degrees of rotation). A triangular-shaped element was then formed by defining the same node number for nodes K, L, and O.

5. Results and discussion

The cut-out was accurately shaped by decreasing the distance gap between the nodes, according to Figure 2. While the circular cut-out is like a square in Figure 2(a) and (b), it is like a circle in Figure 2(d). The con-

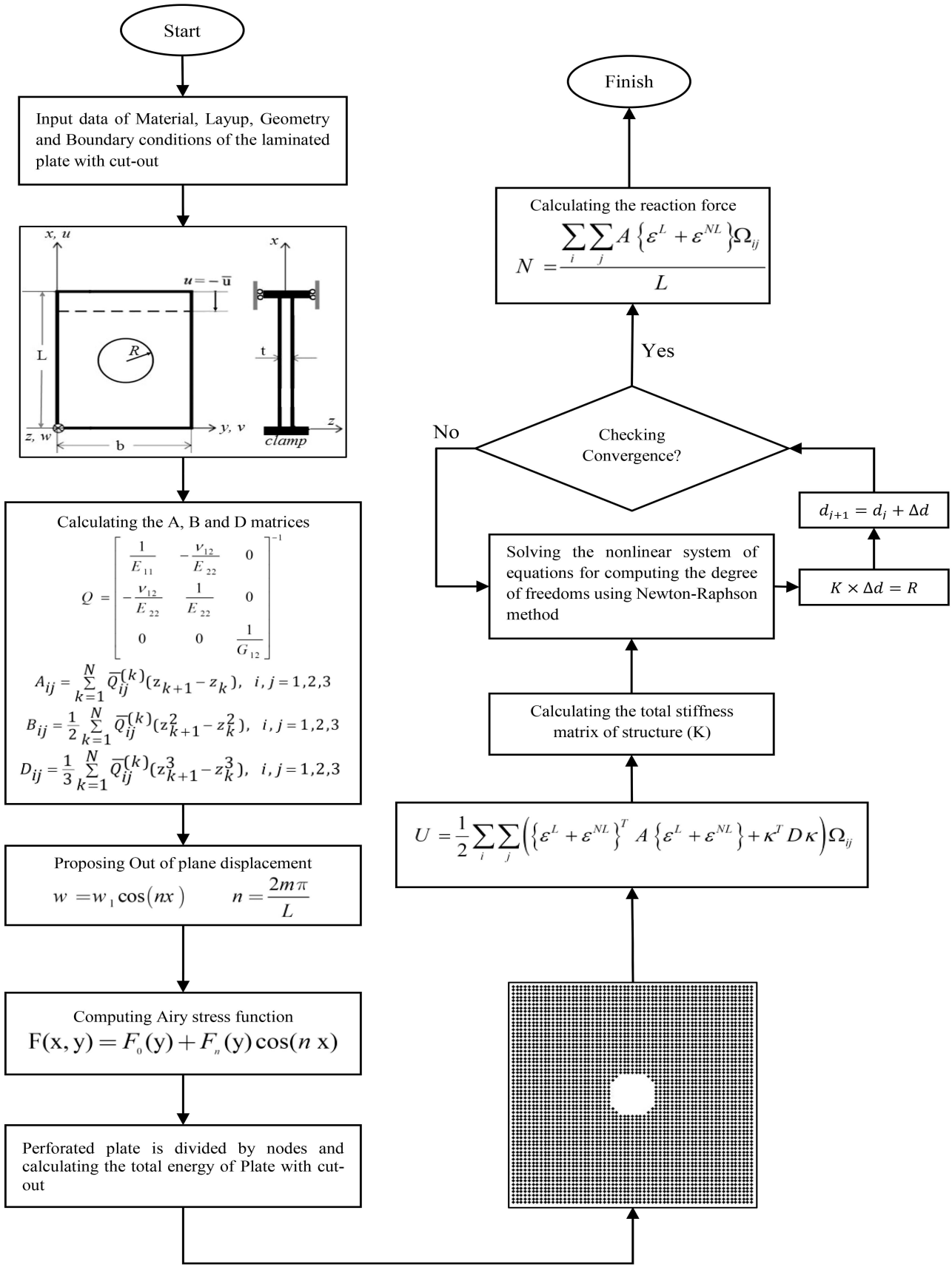

Figure 3. The flowchart of Particle Semi-Energy (PSE) for buckling analysis of composite plate with a cut-out as given in [1].

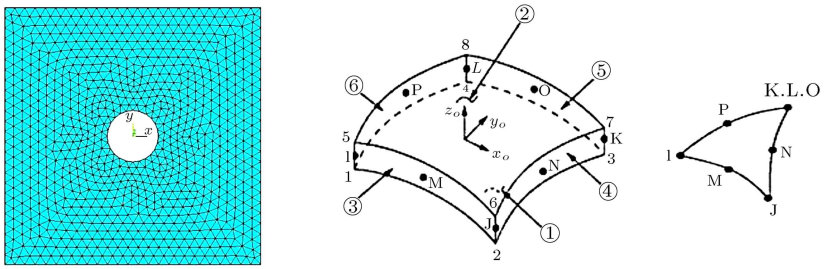

Figure 4. (a) The configuration of the Finite Element Method (FEM) elements shown on a plate with a circular cut-out and a radius of R. (b) The plate element (shell 281) with eight nodes and six degrees of freedom per node.

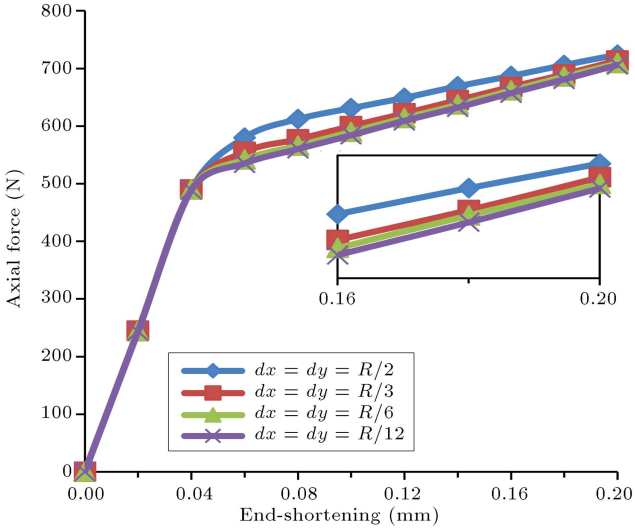

Figure 5. Buckling load convergence of the perforated composite plate with the boundary condition of Figure 1. The plate is $[0.90/0.90]_s$ woven E/glass-epoxy composite with $R = 6$ mm, and $L = b = 60$ mm.

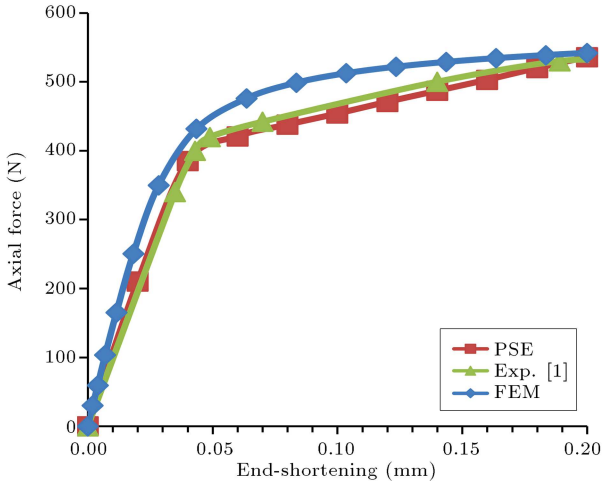

Figure 6. Buckling load of $[0.90/0.90]_s$ woven E/glass-epoxy composite plate with a circular cut-out with the radii of cut-out being 9 mm, and thickness of the plate 0.8 mm.

vergence study of buckling load with a consideration of the distance among the integration nodes on the perforated plate was performed, the results of which are presented in Figure 5. According to the findings, the buckling loads of all node arrangements were close to each other. In addition, the post-buckling behavior of the plate decreased by decreasing the distance gap among the nodes and converges at $R/3$ gap distance.

The post-buckling behavior of a $[0.90/0.90]_s$ woven E/glass-epoxy composite plate was studied using PSE and FEM. The plate had a circular cut-out, and the boundary conditions given in Figure 1 were used in this study. The results obtained from the modelling were compared with the experimental ones [1], as presented in Figure 6, in case the radius of cut-out was 9 mm. The thickness of the plate was 0.8 mm, and the normal elastic modules, shear elastic modules, and Poison's ratio were $E_x = 14.5$ (GPa), $G_s = 5.57$ (GPa), and $v_{xy} = 0.11$ [1], respectively.

The post-buckling behavior of an eight-layered $[0/90]_4$ woven roving glass/epoxy composite plate was studied using PSE and FEM. To this end, it was assumed that the plate did not have a circular cut-out and the boundary conditions of Figure 1 were taken into account. The results of these modeling cases were compared with the experimental ones [23], as presented in Figure 7. The plate thickness was 3 mm, and the normal elastic modules, shear elastic modules, and Poison's ratio were $E_x = 7.4$ (GPa), $G_s = 2.18$ (GPa), and $v_{xy} = 0.17$ [23], respectively.

According to Figures 6 and 7, the buckling load of PSE was in agreement with the experimental results. In the linear parts of the diagrams, the result of FEM solution was better than others. The nonlinear analysis of FEM is based on the buckling mode which was obtained using a linear Eigen-value buckling analysis. Figure 8 shows the displacements of the plate in the buckling mode using FEM. As observed, the in-plane displacement was zero in the buckling mode. Disregarding the transverse displacement of the plate would intensify the axial force of FEM result presented in Figures 6 and 7. In contrast to FEM, PSE finds the in-plane and out-of-plane displacements by minimizing the potential energy at the same time before and after

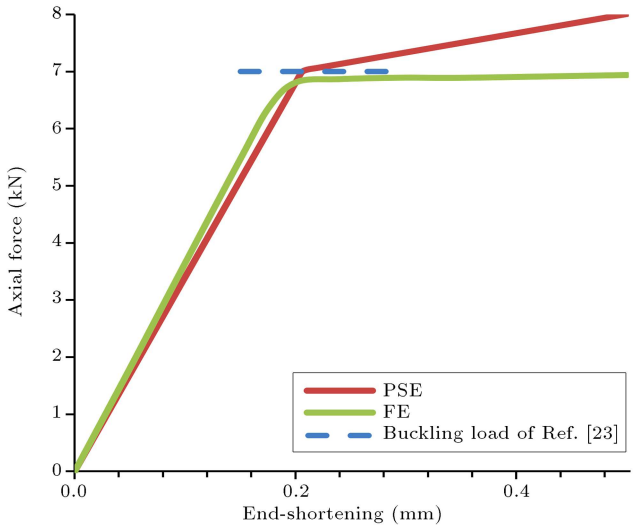

Figure 7. Buckling load of an eight-layered $[0/90]_4$ woven roving glass/epoxy composite plate.

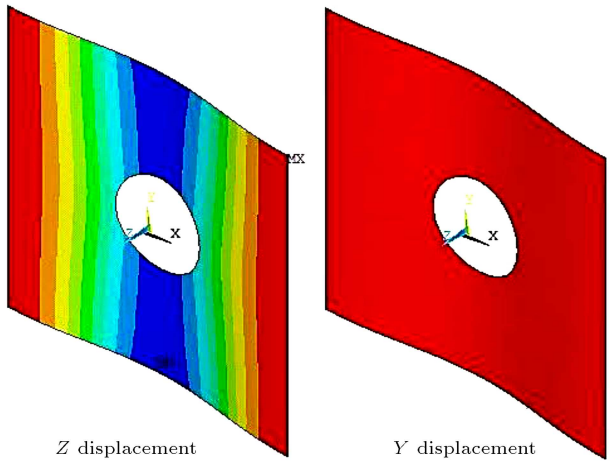

Figure 8. Plate displacements in the buckling mode shape using Finite Element Method (FEM).

the buckling. Therefore, the accuracy of PSE was found higher than that of FEM.

An interesting subject here is the variation of the post-buckling behavior of the composite plate caused by increasing the radius of cut-out. Another comparison was made between the results of FEM and PSE, the results of which are investigated in Figure 9 to evaluate their performance in estimating the buckling force of plates with different cut-outs. Axial forces on the composite plates containing circular cut-outs with diameters of 6 and 9 mm are shown in Figure 9. As expected, the buckling load decreased by increasing the radius of the cut-out. However, the same behavioral pattern was not observed in the FEM results.

Figure 10 shows a composite plate with an elliptical cut-out with πab area at the centre of the plate. The ellipse rotates θ degree along its centre. The dimensions of the plate and cut-outs are $L = 60$, $a = L/6$, and $b = L/12$. In addition, the values for θ are 0°, 30°,

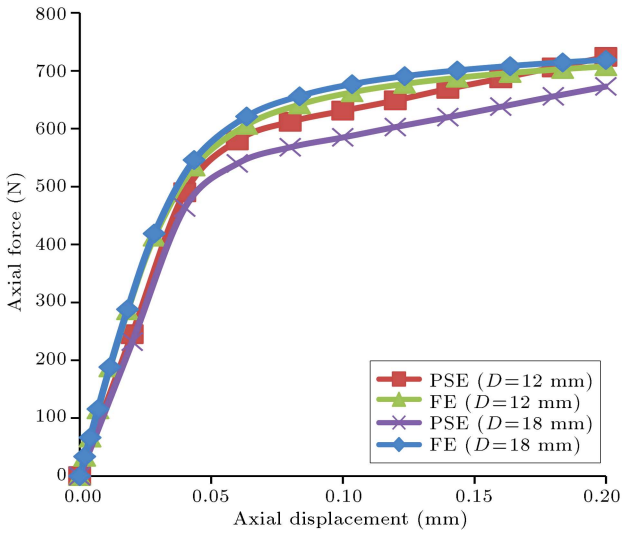

Figure 9. Buckling load of $[0.90/0.90]_s$ woven E/glass-epoxy composite plate with a circular cut-out with the radii of the cut-out being 6 and 9 mm and the thickness of the plate being 0.88 mm.

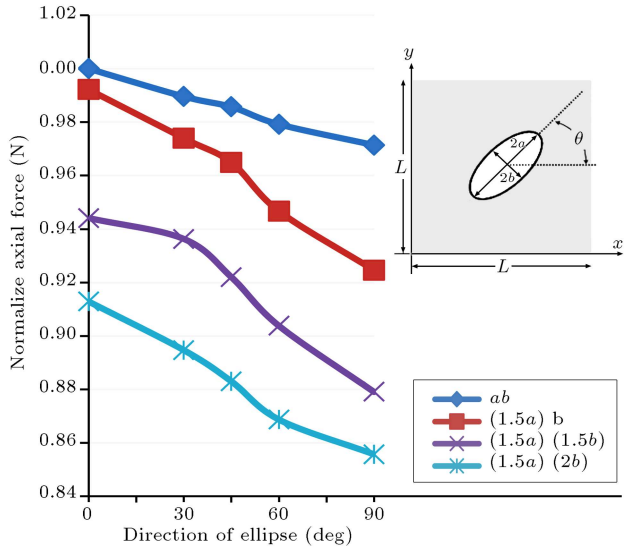

Figure 10. Variation in the post-buckling load of the composite plate including the elliptical cut-out loaded by the end-shortening 0.2 mm and applying Particle Semi-Energy (PSE) method.

45°, 60°, and 90°. The boundary conditions are given in Figure 1. The post-buckling behaviors of this plate were investigated using PSE method with different cut-out dimensions and orientations. The buckling load of plates with different elliptical cut-outs was obtained, while end-shortening loading was 0.2 mm. All these results were normalized by the buckling load of the plate with an elliptical cut-out at $\theta = 0°$. According to this figure, upon increasing θ, the post-buckling load decreased; however, based on Ref. [6], the post-buckling load increased. Different boundary conditions were the main reasons behind these opposite results.

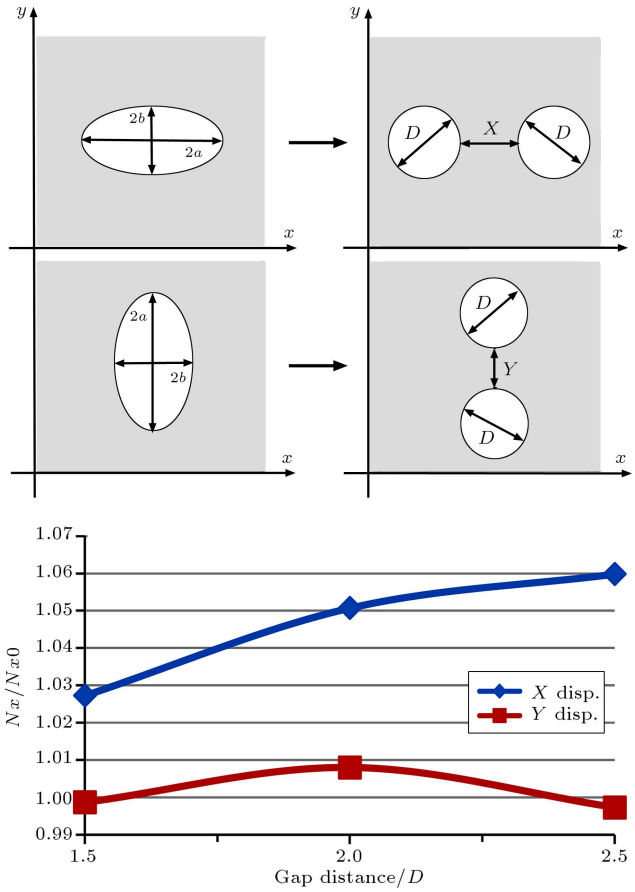

Figure 11. Variation of post-buckling load when an elliptical cut-out is replaced with two circular cut-outs by applying Particle Semi-Energy (PSE) method.

The same phenomenon was observed at the natural frequency of the plate with an elliptical cut-out [24]. In other words, the natural frequency decreased by increasing θ. Based on Figure 10, the total mean force imposed on the composite plate with a big cut-out was the lowest, while the variation for this perforated plate by rotation was the highest. As observed in [25], the natural frequency would decrease by increasing the cut-out size. In addition, upon increasing the cut-out size, the amplitude and period of oscillation of the time-dependent transverse deflection of the laminated plate increased [26].

As shown in Figure 11, an elliptical cut-out was replaced with two circular cut-outs. The areas of the new cut-outs were equal to those of the old one. The distances between these two circles were $1.5D$, $2D$, and $2.5D$, where D is the diameter of the circle. The boundary conditions are given in Figure 1 with the end-shortening capacity being 0.2 mm. The post-buckling load of different arrangements of circles was obtained and normalized by the buckling load of the base plate with an elliptical cut-out. The buckling load of the plate with two horizontal cut-outs was higher than that of the base plate and it increased by widening the gap distance between cut-outs. Increasing the post-buckling load can be seen in a vertical direction while the gap distance is $2D$. The buckling load of the plate with two vertical cut-outs was lower than that of the base plate while the gap distances were $1.5D$ and $2.5D$.

6. Conclusion

The present study aimed to investigate a new technique to calculate the potential energy and buckling load of a composite plate including a circular/elliptical cut-out under end-shortening loading. The stress and strain fields were determined using semi-energy method. The potential energy integrations were replaced by the summations of all nodes on the perforated plate. Moreover, equilibrium equations were obtained using the minimizing potential energy, and unknown displacements were calculated by solving these equations through Newton-Raphson method. The convergence of the new technique, i.e., Particle Semi-Energy (PSE), was studied through different node arrangements. The post-buckling behavior of the perforated composite plate derived from this method was in agreement with the experimental result. In the case of modeling the post-buckling behavior of the plate with the cut-out, the accuracy of PSE was higher than that of Finite Element Method (FEM).

The post-buckling behavior of the plate containing the elliptical cut-out aligned along the direction with θ degree to the axial end-shortening with a boundary condition described in Figure 1 was also analyzed. As observed, the buckling load decreased upon increasing the θ and extending the area of the ellipse. In addition, replacing the axial elliptical cut-out with two circular cut-outs in the same area summation would increase the post-buckling load. Further, increasing the gap distance between two circular cut-outs in the transverse direction does not necessarily lead to increase in the axial load.

Nomenclature

$SE-FSM$	Semi-Energy Finite Strip Method
PSE	Particle Semi-Energy method
FEM	Finite Element Method
ε	Strain vector
ε_x	Normal strain along x direction
ε_y	Normal strain along y direction
ε_{xy}	Shear strain along y direction
ε^L	Linear part of strain vector
ε^{NL}	Non-linear part of strain vector
κ	Curvature of the neutral plane of composite element

A	In-plane stiffness matrix of the composite material
B	Coupling matrix of the forces in- and out-of-plane moments
D	Stiffness matrix of moments and curvatures of the element
F	Airy force function
L	Axial length of the plate
M	Moments per unit length acting on the element component
N	Forces per unit length acting on the element component
$\bar{u}$	End shortening
U	Potential energy
u	Displacement along x direction
v	Displacement along y direction
w	Displacement along z direction
E_x	Normal elastic modules
G_s	Shear elastic modules
v_{xy}	Poisson's ratio

References

1. Shojaee, T., Mohammadi, B., and Madoliat, R. "Development of a finite strip method for efficient prediction of buckling and post-buckling in composite laminates containing a cutout with/without stiffener", *Compos. Struct.*, **210**, pp. 538–552 (2018).
2. Ovesy, H.R., Loughlan, J., and Assaee, H. "The compressive post-local bucking behaviour of thin plates using a semi-energy finite strip approach", *Thin-Walled Struct.*, **42**, pp. 449–474 (2004).
3. Shojaee, T., Mohammadi, B., and Madoliat, R. "Experimental and numerical investigation of stiffener effects on buckling strength of composite laminates with circular cutout", *Journal of Composite Materials*, **54**(9) (2020). DOI: https://doi.org/10.1177/0021998319874101
4. Bash, A.M., Mnawe, S.E., and Salah, S.A. "Numerical buckling analysis of carbon fibre-epoxy composite plates with different cutouts number by finite element method", AIMS *Mater. Sci.*, **7**, pp. 46–59 (2020).
5. Falkowicz, K. and Dębski, H. "Postbuckling behaviour of laminated plates with a cut-out", *Adv. Sci. Technol.*, **11**, pp. 186–193 (2017).
6. Ghannadpour, S.A.M. and Mehrparvar, M. "Energy effect removal technique to model circular/elliptical holes in relatively thick composite plates under in-plane compressive load", *Compos. Struct.*, **202**, pp. 1032–1041 (Oct. 2018). DOI: 10.1016/j.compstruct.2018.05.026
7. Reddy, J.N., *An Introduction to Nonlinear Finite Element Analysis*, Oxford University Press (2004).
8. Assaee, H. and Ovesy, H.R. "A multi-term semi-energy finite strip method for post-buckling analysis of composite plates", *Int. J. Numer. Meth. Engng*, **70**, pp. 1303–1323 (2007).
9. Nemeth, M.P., Stein, M., and Johnson, E.R. "Nemeth, M.P., M. Stein and E.R. Johnson, An approximate buckling analysis for rectangular orthotropic plates with centrally located cutouts", *NASA Tech. Pap.*, 2528 (1986).
10. Kumar, D. and Singh, S.B. "Effects of boundary conditions on buckling and postbuckling responses of composite laminate with various shaped cutouts", *Compos. Struct.*, **92**, pp. 769–779 (2010).
11. Mehrparvar, M. and Ghannadpour, S.A.M. "Plate assembly technique for nonlinear analysis of relatively thick functionally graded plates containing rectangular holes subjected to in-plane compressive load", *Compos. Struct.*, **202**, pp. 867–880 (Oct. 2018). DOI: 10.1016/j.compstruct.2018.04.053
12. Kar, V.R. and Panda, S.K. "Post-buckling behaviour of shear deformable functionally graded curved shell panel under edge compression", *Int. J. Mech. Sci.*, **115**, pp. 318–324 (2016).
13. Mehar, K., Kumar, S., Devarajan, Y., and Choubey, G. "Numerical buckling analysis of graded CNT-reinforced composite sandwich shell structure under thermal loading", *Compos. Struct.*, **216**, pp. 406–414 (2020).
14. Kar, V.R., Panda, S.K., and Mahapatra, T.R. "Thermal buckling behaviour of shear deformable functionally graded single/doubly curved shell panel with TD and TID properties", *Adv. Mater. Res.*, **5**, pp. 205–221 (2016).
15. Katariya, P.V., Panda, S.K., and Mahapatra, T.R. "Nonlinear thermal buckling behaviour of laminated composite panel structure including the stretching effect and higher-order finite element", *Adv. Mater. Res.*, **6**, pp. 349–361 (2017).
16. Mehar, K. and Panda, S.K. "Multiscale modeling approach for thermal buckling analysis of nanocomposite curved structure", *Adv. Nano Res.*, **7**, pp. 179–188 (2019).
17. Kar, V.R., Mahapatra, T.R., and Panda, S.K. "Effect of different temperature load on thermal postbuckling behaviour of functionally graded shallow curved shell panels", *Compos. Struct.*, **160**, pp. 1236–1247 (2017).
18. Kar, V.R. and Panda, S.K. "Postbuckling analysis of shear deformable FG shallow spherical shell panel under nonuniform thermal environment", *J. Therm. Stress.*, **40**, pp. 25–39 (2017).
19. Katariya, P.V. and Panda, S.K. "Thermal buckling and vibration analysis of laminated composite curved shell panel", *Aircr. Eng. Aerosp. Technol. An Int. J.*, **88**, pp. 97–107 (2016).
20. Kumar, S., Pankaj, P., and Katariya, V. "Stability and free vibration behaviour of laminated composite panels under thermo-mechanical loading", *Int. J. Appl. Comput. Math.*, **1**, pp. 475–490 (2015).

21. Katariya, P.V. and Panda, S.K. "Numerical analysis of thermal post-buckling strength of laminated skew sandwich composite shell panel structure including stretching effect", *Steel Compos. Struct.*, **34**, pp. 279–288 (2020).

22. Ovesy, H.R. and Fazilati, J. "Buckling and free vibration finite strip analysis of composite plates with cutout based on two different modeling approaches", *Compos. Struct.*, **94**(3), pp. 1250–1258 (2012).

23. Mohanty, J., Sahu, S.K., and Parhi, P.K. "Numerical and experimental study on buckling behaviour of multiple delaminated composite plates", *Int. J. Struct. Integrity*, **4**, pp. 240–257 (2013).

24. Dewangan, H.C., Panda, S.K., Sharma, N., et al. "Experimental validation of role of cut-out parameters on modal responses of laminated composite-a coupled Fe approach", *Int. J. Appl. Mech.*, **12**(6), 2050068 (2020). DOI: 10.1142/S1758825120500684

25. Dewangan, H.C., Sharma, N., and Hirwani, C.K. "Numerical eigenfrequency and experimental verification of variable cutout (square/rectangular) borne layered glass/epoxy flat/curved panel structure", *Mech. Based Des. Struct. Mach.* (2020). DOI: 10.1080/15397734.2020.1759432

26. Dewangan, H.C., Katariya, P.V., and Panda, S.K. "Time-dependent transverse deflection responses of the layered composite plate with concentric circular cutout", *Materials Today: Proceedings, Elsevier Ltd.*, **33**, Part 8, pp. 4961–4965 (2020). DOI: 10.1016/j.matpr.2020.02.825

Biography

Mohammad Dehghani received his PhD degree from the Yazd University of Iran. He also obtained MSc and BSc degrees from Shahid Chamran University of Ahvaz, Iran. His research interests comprise composite structures, numerical method, finite element method, semi-energy and full-energy finite strip method, smooth particle hydrodynamics method, and theory of elasticity.